A.2.29
972880

A Multi-Fluid CFD Turbulent Entrainment Combustion Model: Formulation and One-Dimensional Results

K. V. Tallio
Powertrain and Vehicle Research Laboratory
Ford Motor Company

P. Colella
Center for Computational Sciences and Engineering
Lawrence Berkeley National Laboratory

Copyright © 1997 Society of Automotive Engineers, Inc.

ABSTRACT

Meeting the increasingly stringent regulations for spark-ignited (SI) internal combustion engines requires understanding the complex chemical and physical processes that occur during combustion. Short time scales and extremes in temperature and pressure make detailed measurements in real combustion systems difficult. To augment the experimental measurements ıumerical models for combustion have been developed. These models can provide insight into the non-linear interactions that occur during combustion and help to guide the design of the system by providing information on parameters that cannot be measured directly.

This paper presents a newly-developed turbulent combustion model that is based on the concepts of the turbulent entrainment model. Quasi-dimensional engine simulations have used models of this type for the past two decades with considerable success. In this study, the model is formulated in a manner suitable for coupling with CFD solvers in one or more spatial dimensions. The existing reaction rate model is retained, but the motion of the entrainment surface is now described using front-tracking techniques. The result is a multi-fluids based turbulent combustion model that incorporates the effects of both the local scale and intensity of the turbulence. The model formulation and preliminary results are presented and discussed.

INTRODUCTION

In this paper, we present a new formulation for implementing the turbulent entrainment combustion model using the multi-fluid algorithms and front-tracking techniques to fully describe the physical processes approximated by this model. As will be discussed below, previous efforts using this combustion model have been limited to zero-dimensional simulations, or modifications to the model's source terms were required to implement it within a multi-dimensional scheme. We have overcome the limitations of previous attempts at a general formulation for the entrainment combustion model and developed an approach that satisfies conservation, correctly predicts the jump in mass, energy and momentum across the flame, retains all of the source terms as originally developed in the model and can be extended to multi-dimensional simulations. One-dimensional results are presented to demonstrate the feasibility of this approach.

Computational models for simulating engine performance have been utilized as part of the engine design process for the last two decades. One-dimensional simulations for gas exchange and quasi-dimensional thermodynamic models for combustion have provided a framework for investigating modifications to existing engines and for evaluating new engine concepts. More advanced models using multi-dimensional computational fluid dynamics (CFD) techniques have seen increasing popularity in recent years due to advances in computational resources. They can now routinely be used to investigate cold flow characteristics within the combustion chamber and to predict conditions at the time of spark [1,2]. However, only in the last several years has it become feasible to apply these simulation tools to model the combustion portion of the engine cycle with full three-dimensional capability [3] .

To date, several different turbulent combustion models have been integrated into multi-dimensional CFD codes for evaluating engine combustion processes . These models range in complexity from the model developed by Branstetter and Johns [4] that solves a full set of transport equations for the reaction progress variable probability density function (PDF) to the mixing controlled

models of Magnuussen [5] where the reaction rate is defined solely by the local turbulent mixing. While the former approach explicitly includes the coupling between the chemistry and turbulent transport, the large number of additional equations required to describe the system makes it very computationally intensive. The latter type of models are formulated with the assumption that the mixing timescales dominate. These models assume that the reaction rate is defined solely by the local turbulent mixing rate and they include no kinetics information. Although mixing models can be adjusted to correctly predict the turbulent burning rate in an integral sense, they are inadequate for computing the instantaneous heat release and hence do not capture the density jump or corresponding compression of unburned gas in front of the flame. In addition, they do not adequately integrate the effects of turbulent scale into the turbulent reaction rate.

Flamelet models represent another class of combustion models used in SI engine combustion simulation. These models are suitable when the chemical timescales are shorter than the corresponding turbulent fluid timescales. The chemical reactions are assumed to occur in thin one-dimensional laminar reaction layers that are embedded in the turbulent flow. The advantage of flamelet models is that they can effectively decouple the chemistry from the calculation of the fluid flow using laminar flamelet libraries that store precomputed laminar flame speed values tabulated as functions of, for example, the unburned thermodynamic state and fluid strain. These models do not explicitly include the effect of turbulent scale on the turbulent reaction rate and they are limited to regimes where the reaction rates are fast relative to the fluid mixing.

Flamelet models can be generally characterized by the method used to transport reactants into the reaction zone. Given that the rate of mass flux of reactants into the reaction zone is defined as the product of the laminar flame speed (S_L) and the unburned gas density (ρ^U), the problem becomes one of modeling the flame surface area and its transport via burning and advection. Flame surface density models, of the type proposed by Cheng and Diringer [6], develop conservation equations for flame surface area that describe its transport, production, and destruction. Wirth and co-workers [7] employ a local field equation formulation to describe the flame surface area. Matthews and colleagues [8-11] use fractal geometry to quantify the flame surface area. This approach accounts for the complete distribution of flame wrinkling scales In addition, instead of using a laminar flame speed library, the unstretched laminar flame speed is computed analytically and the effects of flame strain are included by modifying the local laminar flame speed using an analytical technique similar to the one adopted for the present study.

An alternative to the previously discussed approaches is the turbulent entrainment combustion model. First proposed in the mid-1970's [12] work on this class of combustion models has continued throughout the intervening years [13-18], but has been focused primarily on zero and quasi-dimensional simulations. When incorporated into thermodynamic cycle simulation codes this model provides a means of rapidly evaluating the combustion characteristics of a given engine design. However, as the name implies, quasi-dimensional models include only a minimal description of spatially varying properties and their ability to model many details of the combustion system design is limited. Initial attempts to extend this model to multiple dimensions by Jennings [19] and Bielert and co-workers [20,21] have shown promising results. However, neither group postulated a fully conservative multi-dimensional formulation using the source terms developed as part of the original model.

The entrainment combustion model is phenomenological in nature, but has advantages over both the mixing limited models and the flamelet combustion approach. Unlike the mixing based models, the entrainment model provides a mechanism describing the interaction between the rate of mass consumption by the flame and the rate of heat release that includes chemical kinetics and turbulent scale effects. Flamelet models are restricted to the thin flame regime and assume that burning occurs on a scale that is small relative to the Kolmogorov scale. While Abraham and co-workers [22] demonstrated that this regime may be appropriate for many engine operating conditions, the flamelet model assumptions clearly break down for low engine speeds, cases where high levels of dilution are used for emissions control, and stratified charge operation. The entrainment model, on the other hand, postulates that the appropriate scale for laminar combustion is dictated by the mixing of hot products with fresh charge in the reaction zone, and that this mixing is appropriately characterized by the Taylor microscale of turbulence [13,14]. Groff's [15] experimental measurements in a fan stirred combustion bomb have demonstrated that this approach to modeling turbulent combustion captures the effect of turbulent intensity and length scale on the turbulent flame speed.

In this paper, we present a new formulation for the entrainment combustion model that can be included into simulations for turbulent reacting flows. The present formulation overcomes the limitations of the models developed by Jennings [19] and Bielert and co-workers [20,21]. Utilizing advances in numerical front-tracking techniques [23] and multi-fluid tracking algorithms developed in [24, 25, 26] we have constructed a general engineering model describing the turbulent combustion process that is valid for arbitrary rates of reaction. This model is not intended to provide a means of studying fundamental problems in turbulent combustion, instead it

is an engineering tool that can be applied to evaluate the design of combustion systems for SI engines. While the goal of this work is to ascertain the ability of the entrainment model to predict SI engine combustion, this paper focuses on the formulation of the model. One-dimensional results demonstrate that the model satisfies conservation and correctly captures the jump in energy and momentum across the flame, a necessary step before continuing to higher-order simulations.

COMBUSTION MODEL

The entrainment combustion model represents turbulent flame propagation in two steps. First, turbulent entrainment transports mass into the reaction zone at a rate that is proportional to the local values of laminar flame speed and the turbulence velocity. The freshly entrained mass mixes with the gases already contained in the reaction zone and this mixture is consumed at a rate determined by the concentration of reactants, laminar flame speed and scale of turbulence. Figure 1 shows a conceptual view of the entrainment front as it is used to delineate the entrained and unentrained fluids. Only fluid that has passed through the entrainment front can participate in the combustion reaction and those reactions continue until all of the entrained mass has been converted to products. As such, the initial region behind the entrainment front in this figure represents the reaction zone. All of the gases contained in the region behind the reaction zone are completely burned. Variations in the reaction rate allow the thickness of this zone to vary as a function of space and time due to localized variations in the entrainment velocity, turbulent scale or laminar flame speed.

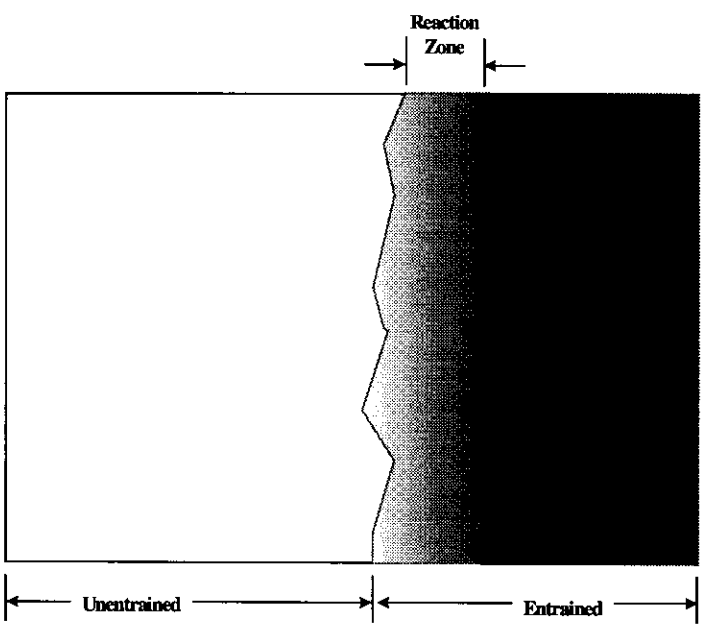

Figure 1. Schematic describing the entrainment combustion process

The entrainment front moves through the combustible mixture at a velocity defined by Blizzard and Keck [12] as:

$$\mathbf{u}_e = (S_L + \beta\, u') \cdot \mathbf{n} \qquad (1)$$

where: $\mathbf{u}_e$ - entrainment velocity
S_L - laminar flame speed
u' - fluctuating velocity
β - model constant
$\mathbf{n}$ - surface normal vector

Based on experimental data, Groff [15] suggests that a value of β=2 is appropriate for the range of turbulence conditions encountered in SI engines. Equation 1 may now be used to define the rate at which mass crosses the entrainment front:

$$\dot{m}_\varepsilon = \rho_u\, \mathbf{u}_e A_f \qquad (2)$$

where: $\dot{m}_\varepsilon$ - entrainment rate
ρ_u - unentrained gas density
A_f - flame area

In contrast to flamelet type models, the flame area used in Eq. 2 is smooth in a sub-grid sense, the effect of flame wrinkling due to turbulence on the mass transport into the flame is included in the entrainment velocity through the u' scaling. Bielert and co-workers [20,21] have demonstrated that the definition of entrainment velocity given in Eq. 1 provides a consistent means of accounting for the increase in flame area due to turbulence. Once the mass crosses the entrainment front it can participate in the combustion reaction. The rate at which this mass is burned is defined [12] as:

$$\dot{m}_b = \frac{m_e - m_b}{\tau} \qquad (3)$$

Here, $\dot{m}_b$ is the rate of mass consumption behind the entrainment front and the time scale, τ, is defined as:

$$\tau = \frac{\alpha\lambda}{S_L} \qquad (4)$$

Where, α is a model constant and, following Tabaczynski and co-workers [14], λ is the Taylor scale of turbulence. Tabaczynski argues that it is the mixing of hot products with the unburned reactants in the entrainment zone that dictates the scale on which laminar burning occurs. Based on this assumption, the appropriate hydrodynamic scale for laminar burning is the Taylor scale.

The model includes the effect of chemical kinetics using correlations for laminar flame speed as a function of

equivalence ratio, temperature, pressure and residual fraction of the type suggested by Rhodes and Keck [27]. Their correlation of experimental data is based on a practical multi-component hydrocarbon fuel, similar to gasoline, and is well suited to the needs of this study. The correlation covers a broad range of equivalence ratios ($0.7 < \phi < 1.6$), pressures ($0.4 < P < 12$ atm), unburned gas temperatures ($350K < T < 550$ K), and residual gas fraction ($0 < f_d < 0.3$) and it takes the form:

$$S_L = S_{Lo}\left(\frac{T_u}{T_o}\right)^A\left(\frac{P}{P_o}\right)^B(1-2.06f_d^{0.733}) \quad (5)$$

where, $S_{L,o}$ is the reference laminar flame speed, in cm/s, measured at T_o=298K and P_o=1 atm and A and B are empirically evaluated coefficients. The reference laminar flame speed is defined as:

$$S_{L,o} = 30.5 - 54.9(\phi - 1.21)^2 \quad (6)$$

and the exponents A and B are defined in terms of the equivalence ratio as:

$$A = 2.4 - 0.271\phi^{3.51}$$
$$B = -0.357 + 0.14\phi^{2.77} \quad (7)$$

't is worthwhile to compare both the average burning rate definition of the entrainment model with that of the flamelet model. Using the relation presented by Khalighi and co-workers [3] for the mean consumption rate of fuel, $\omega_{b,F}$, per unit volume, V, used in the flamelet model formulations:

$$\omega_{b,F} = \rho^U Y_{f,U} S_L \overline{\Sigma} \quad (8)$$

where: ρ^U - unburned gas density
$Y_{f,U}$ - mass fraction of fuel in the unburned gas
$\overline{\Sigma}$ - flame surface area per unit volume

To obtain a direct comparison of Eq. 8 with the entrainment model burn rate it is necessary to normalize Eq. 3 to obtain a burn rate per unit volume. Defining $\omega_{b,\varepsilon}$ as the rate of mass burning per unit volume for the entrainment model and expanding the denominator in Eq. 3 yields:

$$\omega_{b,\varepsilon} = \frac{(\rho^\varepsilon - \rho^b)S_L}{\alpha\lambda} \quad (9)$$

where: ρ^ε- entrained gas density
ρ^b- burned gas density

we recognize that the numerator of this represents the amount of reactants per unit volume behind the entrainment front which is equivalent to the first two terms in Eq 8. The burning rates are equivalent when the following relations are satisfied:

$$\overline{\Sigma} = \frac{1}{\alpha\lambda} \quad (10)$$

or, when the flame surface area per unit volume is, within a constant of proportionality, equal to the reciprocal of the Taylor lengthscale. This illustrates that the burn rate definitions between the flamelet and entrainment model differ only in the choice of lengthscale over which laminar combustion occurs.

The equations presented to this point are the same as those proposed by Tabaczynski and co-workers [13,14] and used for quasi-dimensional simulations. They must be recast in a manner that permits them to be coupled with a full set of conservation equations before being used for to simulate the turbulent combustion process. The next section outlines the development of the governing equations in this form and the methods used to incorporate the entrainment model relations as source terms for these equations.

GOVERNING EQUATIONS AND NUMERICAL TECHNIQUES

Since the purpose of this paper is to present the formulation of, and initial results from, a multi-fluid formulation of the turbulent entrainment combustion model, a simplified form of the governing equations for the fluid flow portion of the problem are adopted. The flow is assumed to be compressible, inviscid and adiabatic with specified turbulent intensity and length scale. These simplifications result in a model that can be compared directly with analytical results. The assumption of specified turbulence quantities introduces no difficulty for these preliminary calculations as the turbulence values are simply an input to the combustion model.

We have adopted the multi-fluid method developed in [24,25] to solve the system of equations presented below. In this model, a compressible fluid may consist of a number of thermodynamically distinct species within a single computational cell. In the formulation used here, only two constituents are considered, entrained and unentrained fluid, but the model is equally valid for an arbitrary number of components. The method utilizes an approach similar to that used for volume-of-fluid (VOF) techniques, the same representation of the fluid is used, but a formal reconstruction of the interface between the fluids is not necessary. This algorithm assumes pressure equilibrium among all of the components within the cell and that a single velocity vector is used

independent of the cell composition. Given the low Mach numbers of these flames the assumption of pressure equilibrium within each computational cell is physically reasonable; however, this does not imply that the pressure is uniform throughout the computational domain.

It is now possible to construct the system of governing equations describing the entrainment model. Conservation of mass for the entrained and unentrained fluid is:

$$\frac{\partial\left(\rho^{\varepsilon} f^{\varepsilon}\right)}{\partial t}+\nabla\cdot\left(\rho^{\varepsilon} f^{\varepsilon}\mathbf{u}\right)=\dot{\omega}_{\varepsilon} \qquad (11)$$

$$\frac{\partial\left(\rho^{U} f^{U}\right)}{\partial t}+\nabla\cdot\left(\rho^{U} f^{U}\mathbf{u}\right)=-\dot{\omega}_{\varepsilon} \qquad (12)$$

$$\frac{\partial\left(\rho^{\varepsilon} f^{\varepsilon} z\right)}{\partial t}+\nabla\cdot\left(\rho^{\varepsilon} f^{\varepsilon} z\mathbf{u}\right)=\dot{\omega}_{b} \qquad (13)$$

where: $\dot{\omega}_{\varepsilon}$ - entrainment rate per unit volume
$\dot{\omega}_{b}$ - burning rate per unit volume
f^{ε} - entrained volume fraction
f^{U} - unentrained volume fraction
z - mass fraction burned

The first two equations describe the rate at which mass is converted from the unentrained to entrained state. The third equation is a description of the rate at which entrained reactants are converted to products of combustion and the transport of these products by advection. The source terms appearing on the right hand side of these equations are defined in a manner that is entirely consistent with the entrainment model.

The energy equations for the entrained and unentrained components take the following form:

$$\frac{\partial\left(\rho^{\varepsilon} f^{\varepsilon} E^{\varepsilon}\right)}{\partial t}+\nabla\cdot\left(\rho^{\varepsilon} f^{\varepsilon} E^{\varepsilon}\mathbf{u}\right)+f^{\varepsilon} p\nabla\cdot\mathbf{u}+\frac{\left(\rho^{\varepsilon} f^{\varepsilon}\right)}{\tilde{\rho}}\mathbf{u}\nabla\cdot p=\dot{\omega}_{\varepsilon}E^{U}+\dot{\omega}_{b}q^{O} \qquad (14)$$

$$\frac{\partial\left(\rho^{U} f^{U} E^{U}\right)}{\partial t}+\nabla\cdot\left(\rho^{U} f^{U} E^{U}\mathbf{u}\right)+f^{U} p\nabla\cdot\mathbf{u}+\frac{\left(\rho^{U} f^{U}\right)}{\tilde{\rho}}\mathbf{u}\nabla\cdot p=-\dot{\omega}_{\varepsilon}E^{U} \qquad (15)$$

where: E^{ξ} - internal energy (= $e+\mathbf{u}^2/2$) of component ξ
p - pressure
q^{o} - fuel energy

The terms on the left hand side of Eq. 14 and 15 describe the advection of energy contained in the entrained and unentrained gases, compression work on or by the gases and flow work, respectively. The right hand side terms account for energy transport across the entrainment front due to mass entrainment and increases in entrained gas energy due to burning. As with the mass transport equations, the source terms are defined to be consistent with the entrainment model definitions.

Finally, conservation of momentum is represented using a single velocity and single density (defined below) as:

$$\frac{\partial\left(\tilde{\rho}\mathbf{u}\right)}{\partial t}+\nabla\cdot\left(\tilde{\rho}\mathbf{u}\mathbf{u}\right)+\nabla\cdot p=0 \qquad (16)$$

The source terms must now be defined in a manner consistent with the entrainment combustion model equations presented previously. The entrainment rate per unit volume describes the rate at which the flame overtakes mass and is defined in terms of the unentrained gas density and the motion of the entrainment front as:

$$\dot{\omega}_{\varepsilon}\equiv\rho^{U}\frac{Df^{\varepsilon}}{Dt} \qquad (17)$$

where the rate of change of entrained volume fraction is evaluated using an eikonal equation for the front motion:

$$\frac{Df^{\varepsilon}}{Dt}=(S_{L}+\beta\, u')\left|\nabla f^{\varepsilon}\right| \qquad (18)$$

The burn rate per unit volume describes the rate at which entrained mass is consumed by the flame and is defined as:

$$\dot{\omega}_{b}=\frac{\rho^{\varepsilon} f^{\varepsilon}(1-z)}{\tau} \qquad (19)$$

The cell pressures are computed as the sum of the partial pressures of the entrained and unentrained constituents in each computational cell. This provides a convenient check to ensure that uniform pressure constraint is satisfied in each computational cell. In cases where the entrained and unentrained pressures do not match, a relaxation scheme is employed to bring them into equilibrium. The partial pressures are defined as:

$$P^{\varepsilon} = \rho^{\varepsilon} (\gamma^{\varepsilon} - 1) e^{\varepsilon} \quad (20)$$

$$P^{U} = \rho^{U} (\gamma^{U} - 1) e^{U} \quad (21)$$

where γ is the ratio of specific heats. For the discussion here, the entrained and unentrained specific heats are assumed to be constant and equal. This assumption is imposed only to simplify the derivations and calculations, later versions will include complete property descriptions.

Finally, constitutive relations and a definition for the laminar flame speed are required to complete the system of equations:

$$f^{\varepsilon} + f^{U} = 1 \quad (22)$$

$$\tilde{\rho} = \rho^{\varepsilon} f^{\varepsilon} + \rho^{U} f^{U} \quad (23)$$

$$P = f^{\varepsilon} P^{\varepsilon} + f^{U} P^{U} \quad (24)$$

Laminar flame speed is determined using a simplified version of the correlation developed by Rhodes and Keck [27] which considers the effects of pressure, temperature, equivalence ratio:

$$S_L = S_{L,o} \left(\frac{T_u}{T_o} \right)^A \left(\frac{P}{P_o} \right)^B \quad (25)$$

The effect of flame stretch can be included in Eq. 25 using a Karlovitz number correction for the laminar flame speed as suggested by Dai and co-workers [16]..

The equations are solved numerically using a fractional step approach. First, the entrainment process is considered. The purpose of this step is to advance the entrainment front due to the intrinsic front velocity.

$$\frac{\partial f^{\varepsilon}}{\partial t} = \frac{\dot{\omega}_{\varepsilon}}{\rho^{U}} \quad (26)$$

The unentrained volume fraction is updated using Eq. 22.

Burning is considered next, using the updated values of entrained mass in each cell computed from the entrainment process, Eq. 19 is used to determine the burning rate. With the entrainment and burning calculations complete, the source terms for the energy equation can be computed and applied to determine the energy state in each cell at the new timestep. In addition to the energy equation, it is also necessary to update the volume fractions in the cells containing the both entrained and unentrained mass. Due to the expansion caused by burning of the entrained gases during the timestep, the values of f^{ε} and f^{U} must be adjusted . To evaluate this effect a pressure form of the first law is used and the pressure equilibrium constraint is invoked. This yields an expression for the change in volume fraction during the burning process that takes the following form:

$$\frac{\partial f^{\varepsilon}}{\partial t} = \frac{f^{U}}{\gamma P} \rho^{\varepsilon} (\gamma - 1) \dot{\omega}_b \quad (27)$$

The sum of Eq (26) and (27) describe the to total change in position of the entrainment front during the entrainment and burning part of the computation:

$$\frac{\partial f^{\varepsilon}}{\partial t} = \frac{\dot{\omega}_{\varepsilon}}{\rho^{U}} + \frac{f^{U}}{\rho^{\varepsilon} p \gamma} \rho^{\varepsilon} (\gamma - 1) \dot{\omega}_b q^{o} \quad (28)$$

This result of the entrainment and burning calculation is used as an input for the multi-fluid advection algorithm to compute the transport terms in each of the differential equations.

This system of equations was solved using an explicit numerical scheme that is second order accurate in space and time. Flux corrected transport techniques were used to limit oscillations in the solution of the fluids portion of the problem caused by steep gradients in density and velocity. Geometric limiters were applied to limit oscillations in the front-tracking calculations.

Prior to presenting results of the simulations further consideration of Eq. 28 is warranted since it possesses some interesting information regarding the model formulation. This equation describes the change in entrained volume fraction due to entrainment and burning for an arbitrary combustion rate. Investigating the properties of this equation for the limiting cases of infinitely fast and infinitely slow kinetics provides some insight into the overall model behavior. In the infinite kinetics limit the entrainment rate and burn rate are equal, as are the entrained and burned density, and the heat input can be replaced with the density jump relation:

$$q^{o} = \frac{\gamma P}{\gamma - 1} \left[\frac{1}{\rho^{b}} - \frac{1}{\rho^{U}} \right] \quad (29)$$

Substituting Eq. 29 into Eq. 28 yields an expression for the change in volume fraction with respect to time for the infinite kinetics limit:

$$\frac{\partial f^{\varepsilon}}{\partial t} = \dot{\omega}_b \left(\frac{\tilde{\rho}}{\rho^{b} \rho^{U}} \right) \quad (30)$$

This describes the motion of the entrainment front when all of the mass is burned instantaneously as it crosses the front and is identically the relationship derived in [28] for an infinite kinetics flame model. At the opposite extreme, that of no kinetics, the second term in Eq. 28 is identically zero and the model describes the kinematics of a discrete traveling front, as expected. These two examples demonstrate that, in the limits of infinitely fast and infinitely slow kinetics, this formulation for the entrainment model is consistent with results obtained by other researchers [e.g., 23, 28] and provides the appropriate framework for describing the motion of the entrainment front.

TEST PROBLEM

Two one-dimensional test problems were selected to evaluate the new model formulation. The first problem considers a flame tube, 100 mm in length, with one end closed and the other open to the atmosphere initially contains a uniform mixture of indolene and air. The first 10 percent of the tube's length is assumed to be both burned and entrained, the entire tube is at uniform pressure. Initially, the velocity everywhere in the flame tube is identically zero. At t=0 the calculations commence and the entrainment front begins to propagate out of the tube entraining and burning mass at rates defined above. The expansion of the gas behind the entrainment front causes the gases to escape the tube at a velocity defined by the front speed and the density ratio of the burned and unburned gas:

$$\mathbf{u}_E = S_F\left(\frac{\rho^U}{\rho^b} - 1\right) \qquad (31)$$

where: $\mathbf{u}_E$ -- expansion velocity
S_F – front speed ($=S_L+\beta u'$)
ρ^b -- burned gas density

Figure 2 depicts the geometry investigated in the test problem and the initial conditions used for the calculations in the first test case.

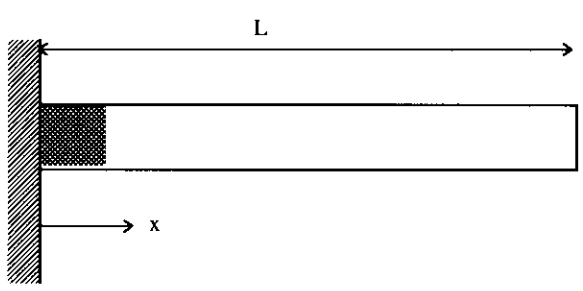

Initial Conditions model constants:

$f^\varepsilon(x<10,0) = 1.0$	$f^\varepsilon(x\geq10,0) = 0.0$
$z(x<10,0) = 1.0$	$z(x\geq10,0) = 0.0$
$\rho(x<10,0) = \rho^b$	$\rho(x\geq10,0) = \rho^U$
$\mathbf{u}(x,0) = 0.0$	$P(x,0) = P_0$
$\alpha = 1.0$	$\beta = 2.0$
$q^0 = 1.8\text{x}10^6$	$\gamma=1.4$

Figure 2. Flame Tube Geometry and Initial Conditions

A one-dimensional combustion bomb is considered for the second test case. Here, the geometries and initial conditions are the same as described above, but the boundary conditions are modified to simulate a fixed volume chamber. For most of the calculations discussed below, 100 computational cells are used to discretize the domain. Higher cell density results are also presented to demonstrate the effect of variations in this parameter on the computed results.

RESULTS AND DISCUSSION

As discussed previously, the model as formulated can provide predictions over a wide range of reaction rates and turbulence levels. The infinitely fast limit for kinetics provides a test case that demonstrates one operating extreme for the model. In this test case the turbulence scale and intensity are set to very small (10^{-8}) values to evaluate the model's ability to capture very sharp gradients and to model this limiting case. Figure 3 shows profiles of f^ε at five different times, the first curve, labeled t=0, is the initial condition used in these calculations and those labeled t=10 ms, t=20 ms, t=30 ms, t=40 ms show the predicted entrainment front position and shape after the calculations have proceeded by the corresponding amount of time. In this and subsequent plots, a value of unity indicates that the fluid has been completely entrained (or burned if z is considered). Notice that the predicted entrainment front maintains its sharp character throughout the duration of the calculation and it is very well defined. The computed results (not shown) verify that profiles for z are coincident with the profiles of f^ε, as expected for the case of infinitely fast kinetics. Figure 4 presents the initial and computed pressure profiles at the same time values presented in the previous figure. When the calculations start, an acoustic pulse is sent out of the tube due to the heat release and resultant local pressure rise in the initially uniform pressure field. Once this initial transient exits the computational domain the pressures profiles are smooth with only small spatial gradients All of the pressure profiles after t=0 are coincident, demonstrating that the system has reached a steady operating condition.

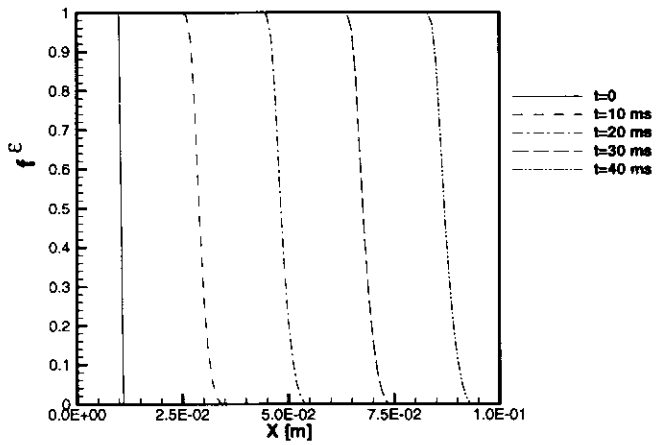

Figure 3. Profiles of Entrained Volume Fraction at Select Times for Infinitely Fast Kinetics in a Flame Tube

In Fig. 5 the velocity profiles produced from the gas expanding due to combustion in the flame tube are shown. Note that the velocity jump through the reaction zone is very well resolved and that it reaches a steady state value of 1.67 m/s, within one percent of the value predicted with Eq. 31. The noise occurring near the maximum velocity profile at 10 ms is a result of initial conditions, the effect of which is reduced in the results for later times. Figure 6 shows the corresponding density profiles. Again, the model captures the rapid change in density that is a result of the infinitely fast combustion considered for this case.

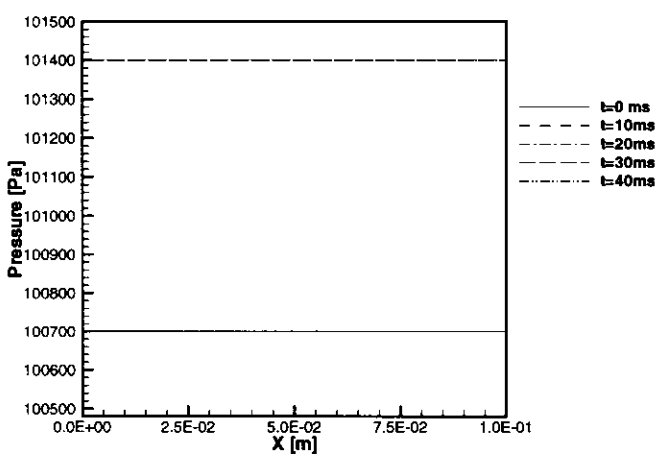

Figure 4. Pressure Profiles at Select Times for Infinitely Fast Kinetics in a Flame Tube

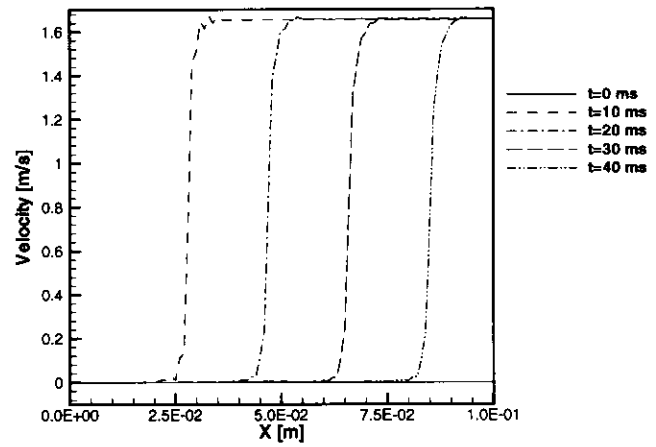

Figure 5. Velocity Profiles at Select Times for Infinitely Fast Kinetics in a Flame Tube

The infinitely fast kinetics predictions show that the model is capable of tracking the sharp fronts that are required for the entrainment model calculations. These

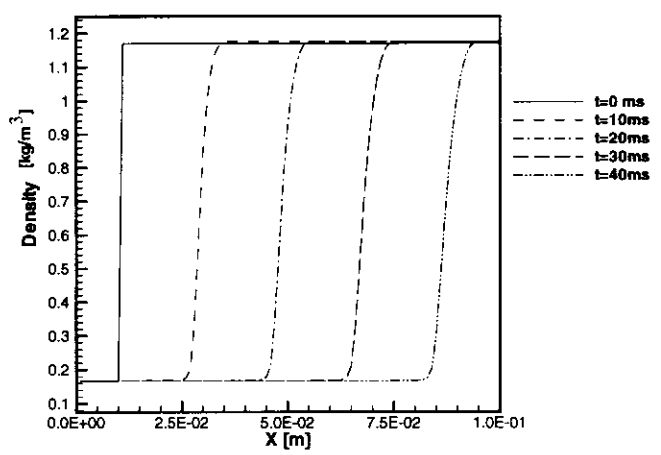

Figure 6. Density Profiles at Select Times for Infinitely Fast Kinetics in a Flame Tube

results also demonstrate that the FCT scheme employed here for the flow field calculations provides a mechanism to resolve the steep gradients in density, velocity and energy. Next, we will demonstrate that the model accurately predicts the burning and expansion velocities for finite rate kinetics. Two test cases are considered to show the effect of turbulence scale and velocity fluctuations on the predicted flame speeds. First, results will be shown for a case with $\lambda=10^{-4}$ m and $u'=10^{-8}$ m/s to demonstrate the effect of changes in turbulent scale. Next, maintaining a value of $\lambda=10^{-4}$ u' will be varied to show its effect on the predictions. Again, the analytical expansion velocity at the tube exit are used as a check for the numerical predictions.

Figure 7 shows the predicted profiles for f^{ε} and z at time t=0 and t=20 ms after the flame is initiated. For comparison, the front speed is fixed at the same value as the infinite kinetics case (i.e., same laminar flame speed and rms velocity) only the turbulent scale parameter is changed from the previous results. In contrast to the infinite kinetics case, two curves are distinctly visible in this figure for the later time results (recall that both f^{ε} and z are coincident at t=0). The entrainment front moves through the reactants at the same rate as before. However, the z profile lags that of f^{ε} due to the finite kinetics time. Velocity profiles at t= 0 and 20 ms are shown in Fig. 8. They exhibit characteristics similar to those for the infinite kinetics case. However, due to the thicker reaction zone the velocities behind the flame do not asymptotically go to zero as rapidly as the previous case. The density profiles shown in Fig. 9, as in the infinite kinetics case the density jump is well resolved, but its width is broadened due to the slower burning.

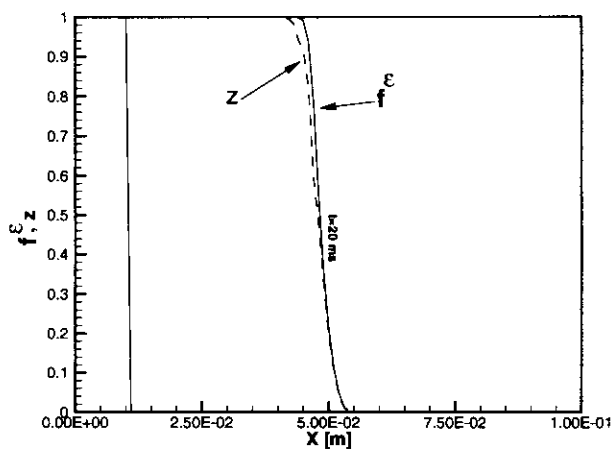

Figure 7. Profiles of Entrained Volume Fraction and Burned Mass Fraction at Select Times for Finite Rate Kinetics in a Flame Tube

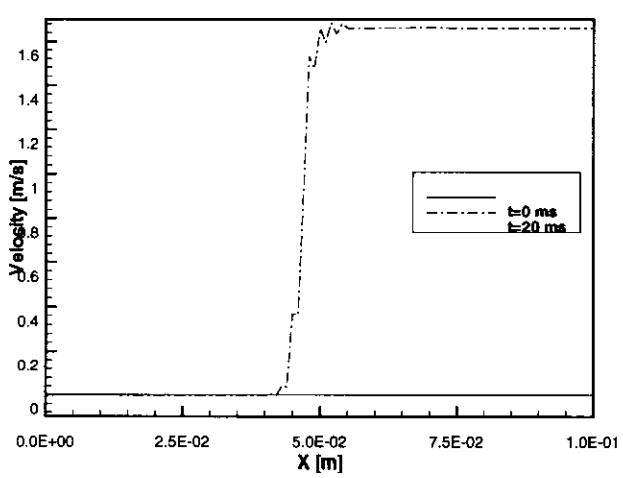

Figure 8. Velocity Profiles at Select Times for Finite Rate Kinetics in a Flame Tube

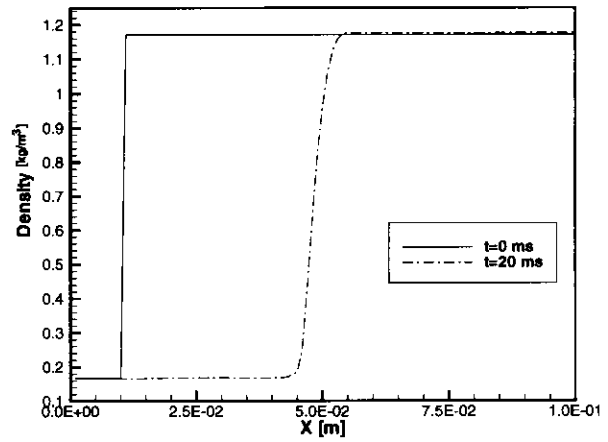

Figure 9. Density Profiles at Select Times for Finite Rate Kinetics in a Flame Tube

The results presented in Fig. 10 demonstrate two properties of the model. Here, the location of the 50 percent volume fraction entrained point is plotted as a function of time for two different rms velocities, 1.0 and 2.0 m/s. After a small non-linear response the entrainment front speed stabilizes and remains constant throughout the calculation. The propagation rate of the entrainment front increases as the turbulence level is increased, as expected, and the mass within the flame tube is consumed at a faster rate for higher levels of turbulence.

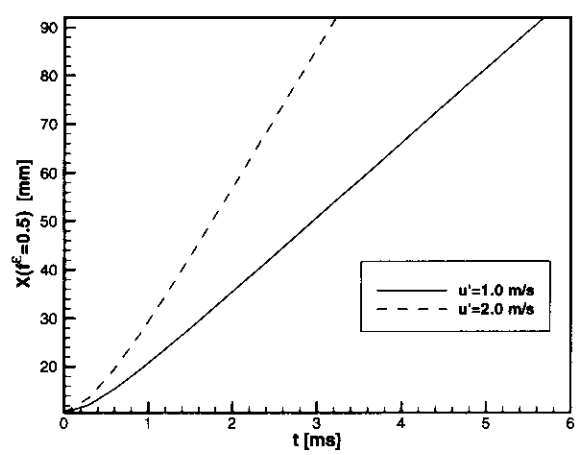

Figure 10. Position of Fifty Percent Volume Fraction Entrained Point as a Function of Time for Two values of rms velocity.

The effect of grid size on the predicted results is shown in Figures 11 through 13. Here, the finite rate kinetics results at t=0 and 20 ms are repeated, but with 1000 computational cells employed. Although admittedly this grid spacing is unrealistic for engineering type

calculations, it is interesting to note that the mean propagation speed of the front is not affected by this parameter. The location of the 50 percent volume fraction entrained point is the same for both calculations. Only the resolution of the front changes. Notice as well that the increased resolution eliminates the noise in the velocity profile observed when only 100 cells were used. We have observed that the numerical technique presented is capable of resolving the entrainment front to within 8 to 12 computational cells for the range of grid spacing demonstrated here, indicating that this technique is well suited to adaptive mesh refinement techniques.

Results for the closed volume calculations are presented in Figures 14 through 17. Here we use the same initial conditions and values for u' and λ as for the finite kinetics case, 100 computational cells are used to discretize the domain. Figure 14 shows the location of the entrainment front and the reaction zone at times of 0 and 20 ms.

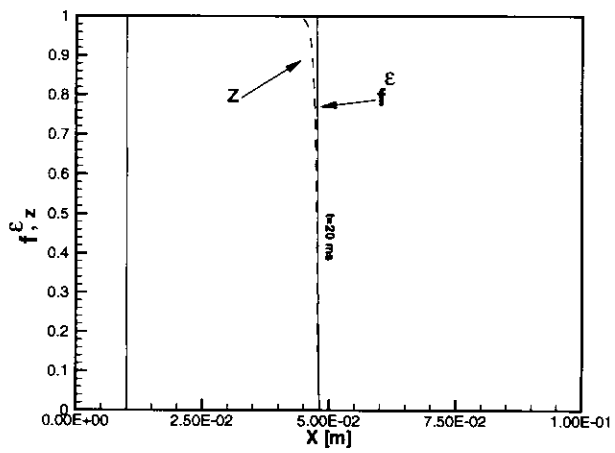

Figure 11. Entrained Volume Fraction and Burned Mass Fraction Profiles at Select Times for High Cell Density Case

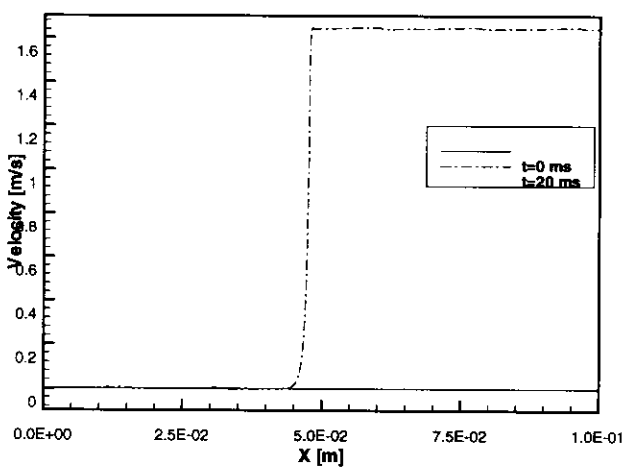

Figure 12. Velocity Profiles at Select Times for High Cell Density Case

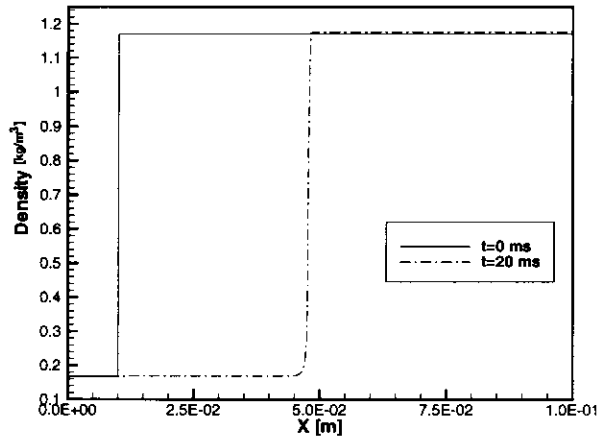

Figure 13.Gas Desity Profiles at Select Times for High Cell Density Case

Notice that both curves are still well resolved and exhibit shapes similar to those observed for the flame tube calculations. However, because these calculations are for a closed volume the fronts do not travel as far as in the open tube case due to the compression of the gases ahead of the front. Figure 15 shows the pressure profiles, the effect of performing the calculations in a closed volume are clearly evident as the pressure has risen significantly. Velocity profiles at 0 and 20 ms are presented in Figure 16. The effect of the combustion generated heat release can be seen in the velocity profile as mass is moving away from the reaction zone to compensate for the rapid change in density. The results of the density calculations can be seen in Figure 17. In these results, unlike those of the open tube case, the density of the unburned gas continues to rise throughout the calculation due to the pressure increase resulting from the constant volume heat release.

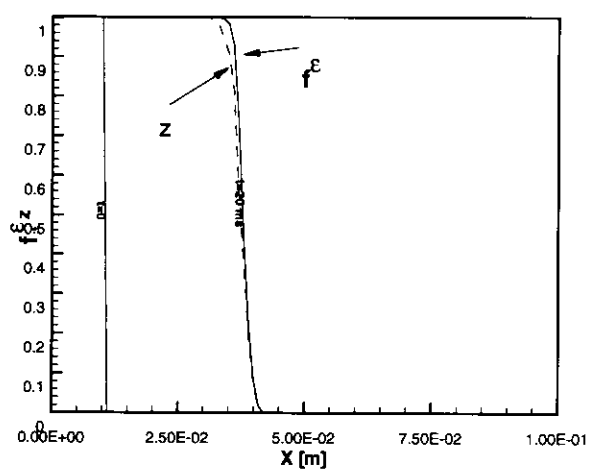

Figure 14. Entrained Volume Fraction and Burned Mass Fraction Profiles at Select Times for Finite Rate Kinetics in a Combustion Bomb

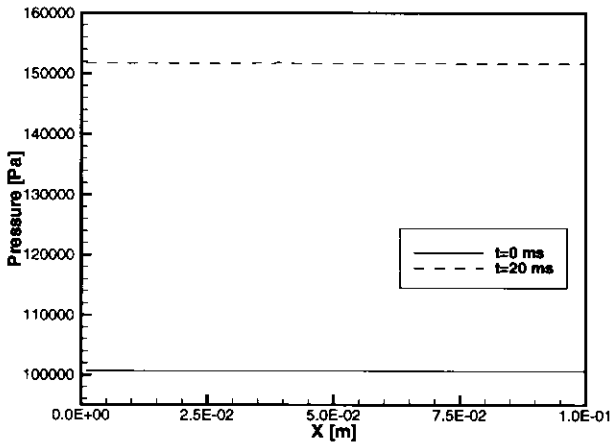

Figure 15. Pressure Profiles as Select Times for Finite Rate Kinetics in a Combustion Bomb

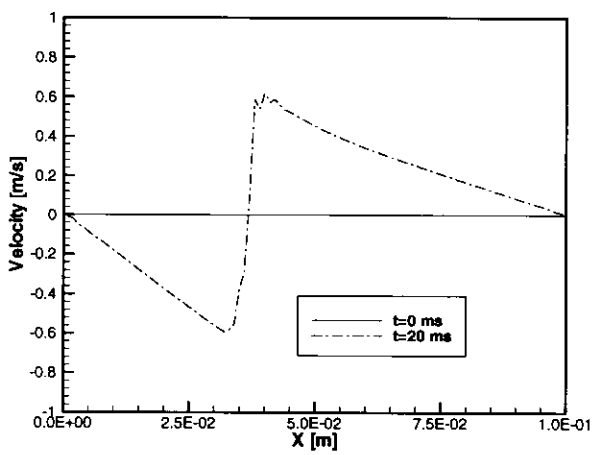

Figure 16. Velocity Profiles at Select Times for Finite Rate Kinetics in a Combustion Bomb

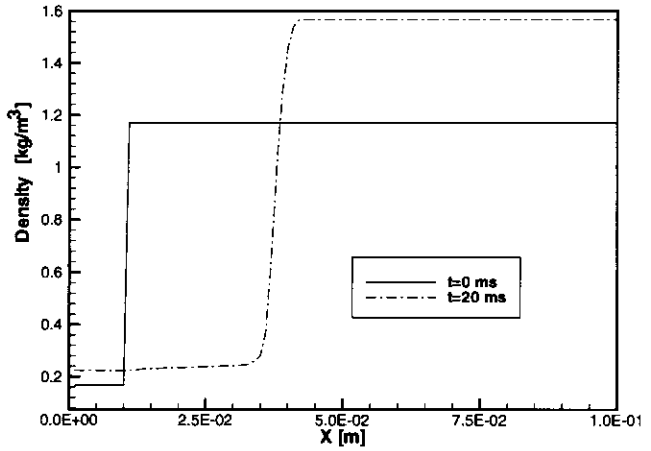

Figure 17. Density Profiles at Select Times for Finite Rate Kinetics in a Combustion Bomb

SUMMARY

We have demonstrated that the mean burn rate models used by both the entrainment and flamelet combustion models are similar, with the difference being the selection of the appropriate scale for laminar burning effects to dominate.

A multi-fluid version of the turbulent entrainment combustion model has been formulated that can be coupled with a CFD model to predict the fluid dynamic effects resulting from the heat released during combustion. Utilizing recent developments in multi-fluid algorithms and front-tracking schemes we have developed a model that overcomes the limitations of previous attempts to incorporate this combustion model into a CFD solver. Unlike past efforts, the method reported here satisfies all conservation laws and implements the combustion related source terms in a manner that is consistent with the assumptions in the turbulent entrainment combustion model. The model represents a general formulation, based on conservation of mass momentum and energy, for variable density front propagation that can be generalized to multiple dimensions.

Preliminary tests on a simple one-dimensional flame tube show that the model predicts the expansion velocity of the flame to within one percent of the analytically determined value, indicating that mass is conserved and the heat release is properly modeled. The rate at which the entrainment front propagates through the combustible mixture reaches a steady value and the model responds as expected to increases in turbulent scale and rms velocity. One-dimensional bomb calculations demonstrate that the model can be applied to closed combustion systems as well. These results have demonstrated that the multi-fluid algorithms and the

front propagation models employed here are capable of accurately predicting the jump in mass, momentum and energy caused by the combustion process.

ACKNOWLEDGMENTS

The authors wish to express their appreciation to Dr. N. Trigui of Ford Motor Company for his support of this project. The assistance, guidance and support provided to the primary author by Professor N.P. Cernansky and the many helpful discussions and suggestions from Dr. R.J. Tabaczynski are gratefully acknowledged. Research at LBNL was supported by the US Department of Energy Mathematical Information, and Computing Sciences Division under contract DE-AC03-76SF00098.

REFERENCES

1. Haworth, D.C., El Tahry, S.H., Huebler, M.S., and Chang, S., "Multidimensional Port-and -Cylinder Flow Calculations for Two- and Four-Valve-Per-Cylinder Engines: Influence of Intake Configuration on Flow Structure," SAE Paper 900257, 1990.
2. Trigui, N., Affes, H., and Kent, J.C., "Use of Experimentally Measured In-Cylinder Flow Field Data at IVC as Initial Conditions to CFD Simulations of Compression Stroke in I.C. Engines - A Feasibility Study," SAE Paper 940280, 1994.
3. Khalighi, B., El Tahry, S.H., Haworth, D.C., and Huebler, M.S., "Computation and Measurement of Flow and Combustion in a Four-Valve Engine with Intake Variations.," SAE paper 950287, 1995.
4. Branstetter W. and Johns, R.J.R., "The Application of a Probability Method to Engine Combustion Modelling," C58/83, IMechE, 1983.
5. Magnussen, B.F. and Hjertager, B.H., "On Mathematical Modeling of Turbulent Combustion with Special Emphasis on Soot Formation and Combustion," *Sixteenth Symposium (International) on Combustion*, The Combustion Institute, pp. 719-729, 1976.
6. Cheng, W.K. and Diringer, J.A., "Numerical Modelling of SI Engine Combustion with a Flame Sheet Model," SAE Paper 910268, 1991.
7. Wirth, M., Keller, P., and Peters, N., "A Flamelet Model for Premixed Turbulent Combustion in SI-Engines," SAE Paper 932646, 1993.
8. Zhu, T.-T., O'Rourke, P.J., and Matthews, R.D., "A Multidimensional Numerical Model for Turbulent Premixed Flames with Fractal Geometries," SAE Paper 952386, 1995.
9. Matthews, T.D., Roberts, C.E., Ellzey, J.L., "SI Engine Modeling Using Fractal Geometry: Promise and Prospects," Proceedings of the KSEA International Technical Conference on Globalization and Technology Frontiers, San Francisco, Sept. 1995.
10. Zhao, X.-W., Matthews, R.D., and Ellzey, J.L., "Three-Dimensional Numerical Simulation of Flame Propagation in Spark-Ignition Engines," SAE Paper 932713, 1993.
11. Zhao, X., Matthews, R.D., and Ellzey, J.L., " Numerical Simulations of Combustion in SI Engines: Comparison of the Fractal Flame Model to the Coherent Flame Model," Proceedings of the Third International Symposium on Diagnostics and Modeling of Combustion in Internal Combustion Engines, JSME/JSAE, pp. 157-162, 1994.
12. Blizzard, N.C. and Keck, J. C. , "Experimental and Theoretical Investigation of Turbulent Burning Model for Internal Combustion Engines," SAE Paper 740191, 1974.
13. Tabaczynski, R. J., Ferguson, C. R., and Radhakrishnan, K.,. "A Turbulent Entrainment Model for Spark-Ignition Engine Combustion," SAE Paper 770647, 1977.
14. Tabaczynski, R. J., Trinker, F. H., and Shannon, B. A. S., "Further Refinement and Validation of a Turbulent Flame Propagation Model for Spark-Ignition Engines," *Combustion and Flame*, vol. 39, pp. 111-121, 1980.
15. Groff, E.G., "An Experimental Evaluation of an Entrainment Flame-Propagation Model," *Combustion and Flame*, Vol. 67, pp. 153-162, 1987.
16. Dai, W., Davis, G.C., Hall, M.J., and Matthews, R. D., "Diluents and Lean Mixture Combustion Modeling for SI Engines with a Quasi-Dimensional Model," SAE Paper 952382, 1995.
17. Brehob, D.D. and Newman, C.E., "Monte Carlo Simulation of Cycle by Cycle Variability," SAE Paper 922165, 1992.
18. Morel, T., Rackmil, C.I., Keribar, R., and Jennings, M.J. , "Model for Heat Transfer and Combustion in Spark Ignited Engines and its Comparison with Experiments," SAE Paper 880198, 1988.
19. Jennings, M. J., "Multi-Dimensional Modeling of Turbulent Premixed Charge Combustion" SAE Paper 920589, 1992.
20. Bielert, U., Klug, M. and Adomeit, G., "Application of Front Tracking Techniques to the Turbulent Combustion Processes in a Single Stroke Device.," *Combustion and Flame*, vol. 106, pp. 11-28, 1996.
21. Bielert, U., Klug, M., and Adomeit, G., "Numerical Simulation of the Turbulent Combustion Process in a Rapid Compression Device," SAE paper 940211, 1994.

22. Abraham, J., Williams, F.A., and Bracco, F.V., "A Discussion of Turbulent Flame Structure in Premixed Charges.," SAE Paper 850345, 1985

23. Osher, S. and Sethian, J.A. , "Fronts Propagating with Curvature-Dependent Speed: Algorithms Based on Hamilton-Jacobi Formulations," *J. Computational Physics,* Vol. 79, pp. 12-49, 1988.

24. Greenough, J.A., Beckner, V., Pember, R.B., Crutchfield, W.Y., Bell, J.B., and Colella, P. "An adaptive multifluid interface-capturing method for compressible flow in complex geometries." Proceedings of the 12th AIAA CFD Conference, San Diego, CA, June 19-22, 1995

25. Greenough, J.A., Bell, J.B., and Colella, P. "An adaptive multifluid interface-capturing method for compressible flow." submitted to the *J. Computational Physics.*

26. Bell, J.B., Colella, P., Greenough, J.A., and Marcus, D. " A Multifluid Algorithim for Compressible Reacting Flows." Proceedings of the 12th AIAA CFD Conference, San Diego, CA, June 19-22, 1995.

27. Rhodes, D.B. and Keck, J.C. "Laminar Burning Measurements of Indolene-Air-Diluent Mixtures at High Pressures and Temperatures," SAE Paper 850047, 1985.

28. Colella, P. " A Multifluid Algorithim for Compressible Reacting Flows.," Sixth International Symposium on Numerical Combustion, New Orleans, LA., 1996.